Cell Reports

Report

Innate Sensing through Mesenchymal TLR4/MyD88 Signals Promotes Spontaneous Intestinal Tumorigenesis

Graphical Abstract

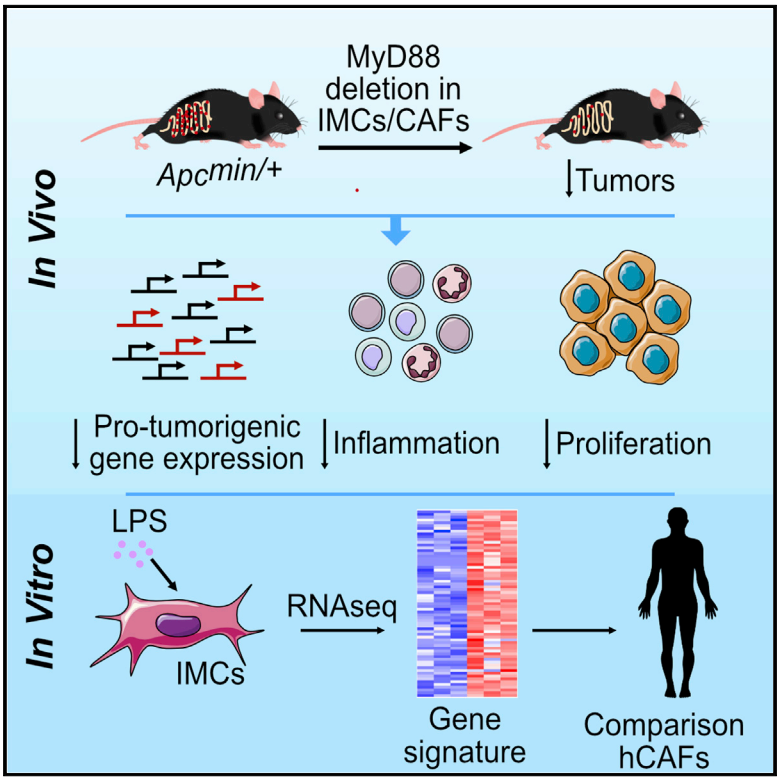

Highlights

- Deletion of MyD88 or TLR4 in IMCs and/or CAFs leads to reduced intestinal tumorigenesis
- The phenotype of the IMC-specific MyD88 mice is similar to the complete knockouts
- MyD88$^{-/-}$ IMCs show a reduced pro-tumorigenic and/or inflammatory gene expression profile
- Human CAFs show upregulation of a similar MyD88-specific gene expression signature

Authors

Vasiliki Koliaraki, Niki Chalkidi, Ana Henriques, ..., David J. Hackam, Manolis Pasparakis, George Kollias

Correspondence

koliaraki@fleming.gr (V.K.), kollias@fleming.gr (G.K.)

In Brief

Koliaraki et al. show that MyD88 in mesenchymal cells is responsible for its tumor-promoting role in the *Apc*$^{min/+}$ model. They further show that this is a TLR4-mediated mechanism that leads to the production of pro-tumorigenic molecules, also identified in human CAFs.

Koliaraki et al., 2019, Cell Reports *26*, 536–545
January 15, 2019
https://doi.org/10.1016/j.celrep.2018.12.072

CellPress

OPEN ACCESS
CellPress

Cell Reports
Report

Innate Sensing through Mesenchymal TLR4/MyD88 Signals Promotes Spontaneous Intestinal Tumorigenesis

Vasiliki Koliaraki,[1,*] Niki Chalkidi,[1] Ana Henriques,[1] Christos Tzaferis,[1] Apostolos Polykratis,[2] Ari Waisman,[3] Werner Muller,[4] David J. Hackam,[5,6] Manolis Pasparakis,[2] and George Kollias[1,7,8,*]

[1]Biomedical Sciences Research Centre (BSRC) "Alexander Fleming," Vari 16672, Greece
[2]Institute for Genetics, University of Cologne, Cologne 50674, Germany
[3]Institute for Molecular Medicine, University Medical Center of the Johannes Gutenberg University Mainz, Mainz 55131, Germany
[4]Faculty of Biology, Medicine and Health, University of Manchester, Manchester M139PT, UK
[5]Division of Pediatric Surgery, Department of Surgery, Johns Hopkins University School of Medicine, Baltimore, MD 21287, USA
[6]The Bloomberg Children's Center, Baltimore, MD 21287, USA
[7]Department of Physiology, Medical School, National and Kapodistrian University of Athens, Athens 11527, Greece
[8]Lead Contact
*Correspondence: koliaraki@fleming.gr (V.K.), kollias@fleming.gr (G.K.)
https://doi.org/10.1016/j.celrep.2018.12.072

SUMMARY

MyD88, an adaptor molecule downstream of innate pathways, plays a significant tumor-promoting role in sporadic intestinal carcinogenesis of the *Apc*$^{min/+}$ model, which carries a mutation in the *Apc* gene. Here, we show that deletion of MyD88 in intestinal mesenchymal cells (IMCs) significantly reduces tumorigenesis in this model. This phenotype is associated with decreased epithelial cell proliferation, altered inflammatory and tumorigenic immune cell infiltration, and modified gene expression similar to complete MyD88 knockout mice. Genetic deletion of TLR4, but not interleukin-1 receptor (IL-1R), in IMCs led to altered molecular profiles and reduction of intestinal tumors similar to the MyD88 deficiency. *Ex vivo* analysis in IMCs indicated that these effects could be mediated through downstream signals involving growth factors and inflammatory and extracellular matrix (ECM)-regulating genes, also found in human cancer-associated fibroblasts (CAFs). Our results provide direct evidence that during tumorigenesis, IMCs and CAFs are activated by innate TLR4/MyD88-mediated signals and promote carcinogenesis in the intestine.

INTRODUCTION

Intestinal carcinogenesis is the result of multiple mutations, but it is now well established that the microenvironment plays also an important role in cancer growth, progression, and metastasis (Hanahan and Coussens, 2012). One of the most important deregulated pathways in intestinal cancer is the β-catenin pathway. In mice, mutation in the *Apc* gene, a central regulator of β-catenin signaling, leads to spontaneous intestinal carcinogenesis similar to human familial adenomatous polyposis, characterized by multiple polyps located mainly in the small intestine (*Apc*$^{min/+}$ model) (Dove et al., 1997). The difference in tumor location between mice and humans is due to the different number of stem cell divisions in the colon and small intestine between the two species (Tomasetti and Vogelstein, 2015). Antibiotic treatment or rederivation of *Apc*$^{min/+}$ mice in germ-free conditions results in reduced tumor load, indicating an important tumor-promoting role of the microbiota in intestinal tumorigenesis (Dove et al., 1997; Li et al., 2012; Song et al., 2014). This is mechanistically associated with increased c-Jun and signal transducer and activator of transcription 3 (STAT3) phosphorylation in cancer cells and increased infiltration of inflammatory cells (Li et al., 2012).

MyD88 is a central regulator of innate immunity, as it acts directly downstream of Toll-like receptors (TLRs) and cytokine receptors, while it is also implicated in carcinogenesis (Salcedo et al., 2013). Genetic deletion of MyD88 in *Apc*$^{min/+}$ mice results in reduced number and size of tumors and correlates with suppressed proliferation, enhanced apoptosis, and a deregulated gene expression profile in tumors (Rakoff-Nahoum and Medzhitov, 2007). Bone marrow chimeras have shown that polyp growth in *Apc*$^{min/+}$ mice depends on MyD88 signaling in non-hematopoietic cells, and MyD88 in intestinal epithelial cells (IECs) was shown to stabilize Myc expression through ERK phosphorylation (Lee et al., 2010).

The role of intestinal mesenchymal cells (IMCs) in inflammation and cancer has recently gained momentum. The ability of IMCs to respond to inflammatory stimuli and regulate immune responses and inflammation has been demonstrated *in vitro*; however, its pathophysiological significance has only recently started to be characterized (Koliaraki et al., 2017; Powell et al., 2011). We have recently dissected intracellular MAPK

and nuclear factor κB (NF-κB) signals that modulate the function of IMCs in the development of colitis and colitis-associated cancer (Henriques et al., 2018; Koliaraki et al., 2012, 2015; Roulis et al., 2014). In the present study, we explored the *in vivo* role of mesenchymal-specific innate sensing in spontaneous intestinal tumorigenesis of the $Apc^{min/+}$ mouse model. We reveal that TLR4/MyD88 signaling in IMCs and/or CAFs is a dominant physiological mechanism in the promotion of cancer.

RESULTS

MyD88 Signaling in Mesenchymal Cells Promotes Intestinal Tumorigenesis in the $Apc^{min/+}$ Model

Since IMCs have been shown to respond to immune stimuli *in vitro*, we hypothesized that IMCs could play a significant role in intestinal carcinogenesis via sensing of innate stimuli. To examine the pathophysiological role of IMC-specific MyD88 in disease pathogenesis of the $Apc^{min/+}$ model, we crossed MyD88 conditional knockout mice with ColVI-cre mice ($Apc^{min/+}$-$Myd88^{IMCko}$), which target mesenchymal cells in the intestine and intestinal tumors (Armaka et al., 2008; Koliaraki et al., 2015). Deletion efficiency in $ColVI^{+}$ cells was verified by qRT-PCR analysis (Figure S1A). 4-month-old $Apc^{min/+}$-$Myd88^{IMCko}$ mice displayed a significant reduction in both the number and size of tumors in comparison to their littermate $Apc^{min/+}$-$Myd88^{F/F}$ controls (Figures 1A–1D). Stratification of tumor frequency by intestinal region showed that the differences were mainly found in the small intestine and particularly in the ileum and jejunum, where the majority of polyps are also located (Figure 1B). It should be noted that Cre itself did not affect tumor development (Figures S2A and S2B). In addition, size-matched tumors from the $Apc^{min/+}$-$Myd88^{IMCko}$ mice showed decreased proliferation, while there was no difference in apoptosis, assessed by bromodeoxyuridine (BrdU) incorporation and Tunel staining, respectively (Figures 1E–1G). Histopathological analysis at 6 weeks of age did not show a statistically significant decrease in the number of dysplastic foci in the small intestine of $Apc^{min/+}$-$Myd88^{IMCko}$ mice, suggesting a more important role for IMC-specific MyD88 in the progression rather than initiation of carcinogenesis, which is consistent with the role of MyD88 in this model (Rakoff-Nahoum and Medzhitov, 2007) (Figure 1H).

Contrary to spontaneous tumorigenesis, mesenchymal-specific deletion of MyD88 did not have a significant effect in the azoxymethane (AOM)/dextran sulfate sodium (DSS) model of inflammation-induced colorectal carcinogenesis (Figure 1I). These results suggest an important tumor-promoting role of the MyD88 signaling pathway in IMCs in spontaneous intestinal tumorigenesis and are in agreement with the phenotype of complete MyD88 knockout mice in this model, which show a significant reduction in tumor load, accompanied by reduced proliferation (Rakoff-Nahoum and Medzhitov, 2007). Differences in the severity of the disease, apoptosis, and the effect on colonic polyps between the complete and conditional knockout mice indicate that MyD88 in other stromal cell types, including other mesenchymal cell populations, could also contribute to the phenotype of the complete MyD88 knockout mice.

Deletion of MyD88 in IMCs Results in Deregulated Gene Expression, Reduced STAT3 Phosphorylation, and Altered Inflammatory Cell Infiltration

To further analyze the similarities between $Apc^{min/+}$-$Myd88^{IMCko}$ mice and the complete knockout mice, we next analyzed the gene expression profile of $Apc^{min/+}$-$Myd88^{IMCko}$ tumors by measuring the expression level of genes that were differentially regulated in the complete MyD88 knockout mice (Rakoff-Nahoum and Medzhitov, 2007). We found significant deregulation in many genes, especially those encoding pro-inflammatory mediators and matrix metalloproteinases (MMPs), while *Igf1* and *Igfbp5* were not upregulated in our tumor samples (Figure 2A). Interestingly, among the deregulated genes were *Il6* and *Il11*, two pro-inflammatory cytokines with important functions in enhancing epithelial cell proliferation and tumorigenesis through STAT3 activation (Bollrath et al., 2009; Schmidt et al., 2018). Accordingly, we found that $Apc^{min/+}$-$Myd88^{IMCko}$ mice showed decreased pSTAT3 staining both in tumors and normal villi in comparison to $Apc^{min/+}$-$Myd88^{F/F}$ controls (Figures 2B and 2C). Since there was a significant differential expression of pro-inflammatory genes in the small intestine of $Apc^{min/+}$-$Myd88^{IMCko}$ mice, we also examined inflammatory cell infiltration in tumors by fluorescence-activated cell sorting (FACS) analysis. We did not find statistically significant differences in the numbers of infiltrating $CD45^{+}$ hematopoietic cells between the two genotypes (Figure 2D); however, we found a reduction in $CD45^{+}CD11b^{+}F4/80^{+}$ macrophages, $CD45^{+}CD11b^{+}Gr1^{+}$ neutrophils, and $CD45^{+}CD4^{+}$ T cells, while $CD45^{+}CD8^{+}$ T cells were increased in the $Apc^{min/+}$-$Myd88^{IMCko}$ tumors (Figures 2E and 2F; Figure S3A). There was no statistically significant difference in the normal small intestine between the two genotypes (Figure S3B). Therefore, $Apc^{min/+}$-$Myd88^{IMCko}$ mice display altered balances in immune infiltration toward a less pro-inflammatory microenvironment and interestingly enhanced cytotoxic T cell infiltration, both being directly associated with the decreased number and size of tumors. These results indicate that a MyD88-dependent pathway in IMCs and/or CAFs regulates the infiltration of immune populations creating a pro-tumorigenic inflammatory milieu in the $Apc^{min/+}$ model, which potentially acts as an additional mechanism to accelerate tumorigenesis.

Importantly, deletion of MyD88 did not influence the distribution of $ColVIcre^{+}$ cells in tumors of the $Apc^{min/+}$-$Myd88^{IMCko}$ mice, as assessed by combining these mice with the $Rosa^{mT/mG}$ (mT/mG) reporter mice, suggesting that MyD88 signaling does not interfere with normal development of these cells (Figure 2G). The specificity of the ColVI-cre mouse for IMCs and/or CAFs in tumors was also verified by FACS analysis, using the lineage-negative markers epithelial cell adhesion molecule (EpCAM), cluster of differentiation 45 (CD45), and CD31 for epithelial, immune, and endothelial cells, respectively (Figures 2H and S3C).

IMC-Specific Genetic Deletion of TLR4, but Not IL-1R, Reduces Tumorigenesis in the $Apc^{min/+}$ Model

To further identify the innate molecular mechanisms regulated by MyD88 in IMCs, we next isolated mesenchymal cells from the small intestine and incubated them with various MyD88

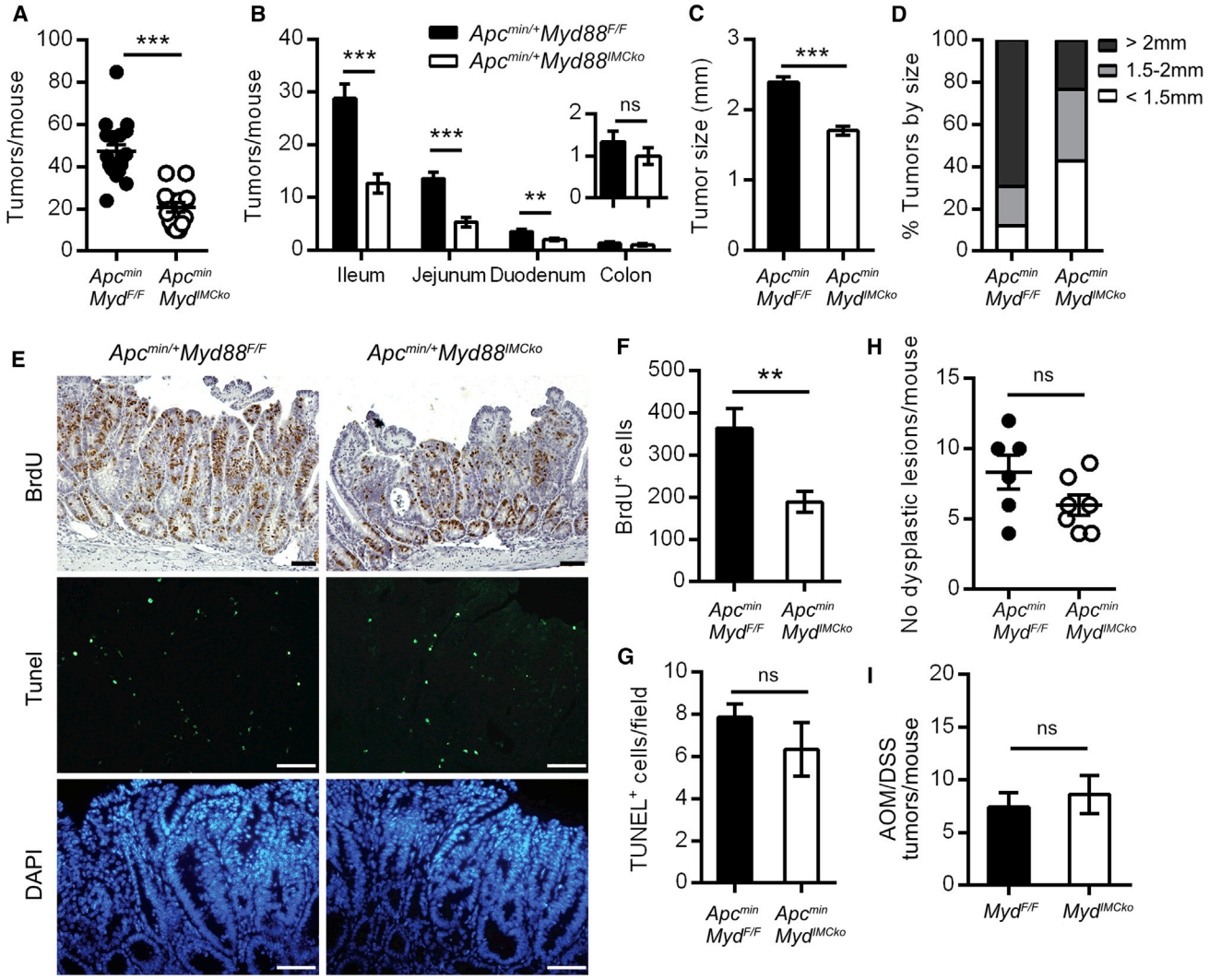

Figure 1. Deletion of MyD88 in Intestinal Mesenchymal Cells Reduces Tumorigenesis in the *Apc*$^{min/+}$ Model of Sporadic Intestinal Cancer

(A and B) Total number of tumors per mouse (A) and number of tumors per intestinal part (B) in 4-month-old *Apc*$^{min/+}$*Myd88*^{IMCko} mice (n = 15) and their littermate controls (n = 18). The insert shows the number of colonic tumors.

(C and D) Size of small intestinal tumors presented as mean tumor size (C) and distribution of tumors per size (D) in the two genotypes.

(E) Representative BrdU and Tunel staining in small intestinal tumors of *Apc*$^{min/+}$*Myd88*^{IMCko} mice and their littermate controls. DAPI was used to stain the nuclei in the Tunel stainings.

(F and G) Quantification of the number of BrdU^{+} cells per tumor (F) and Tunel^{+} cells (G) per field in equal-sized tumors (n = 6 mice per genotype).

(H) Number of dysplastic lesions per mouse in 6-week-old *Apc*$^{min/+}$*Myd88*^{IMCko} and their littermate controls (n = 6–7 mice per genotype).

(I) Number of tumors per mouse in *Myd88*^{IMCko} mice (n = 8) and their littermate controls (n = 7) at the end of the AOM/DSS protocol (one representative experiment of four performed).

Data represent mean ± SEM. **p < 0.01, ***p < 0.001, ns = not significant. Scale bars represent 50 μm. See also Figures S1 and S2.

inducers, including TLR ligands and interleukins IL-1β (interleukin-1β), IL-18, and IL-33. We used measurement of IL-6 as the readout of this initial analysis. Our results showed that IL-6 was increased in response to IL-1β and ligands for TLR1/2, TLR4, and TLR6 and that lipopolysaccharide (LPS) and IL-1β were the stimuli that produced the most abundant effect (Figure 3A). Moreover, analysis of the dataset GEO: GSE39395, which contains expression profiles of isolated cancer cells, leukocytes, and cancer-associated fibroblasts from tumors of patients with colorectal cancer, revealed enrichment in genes encoding *TLR4* and *TLR5*, as well as receptors for the cytokines IL-1 and IL-33 (*IL1R1*, *IL1RL1*, and *IL1RAP*) in CAFs versus cancer cells or leukocytes (Figure 3B) (Calon et al., 2012).

Based on this analysis, we focused more on LPS and IL-1β stimulation. LPS is known to activate innate immune responses in IMCs *in vitro*, leading to production of pro-inflammatory molecules, such as IL-6, COX2, and CXCL1, through activation of several signaling pathways, including NF-κB,

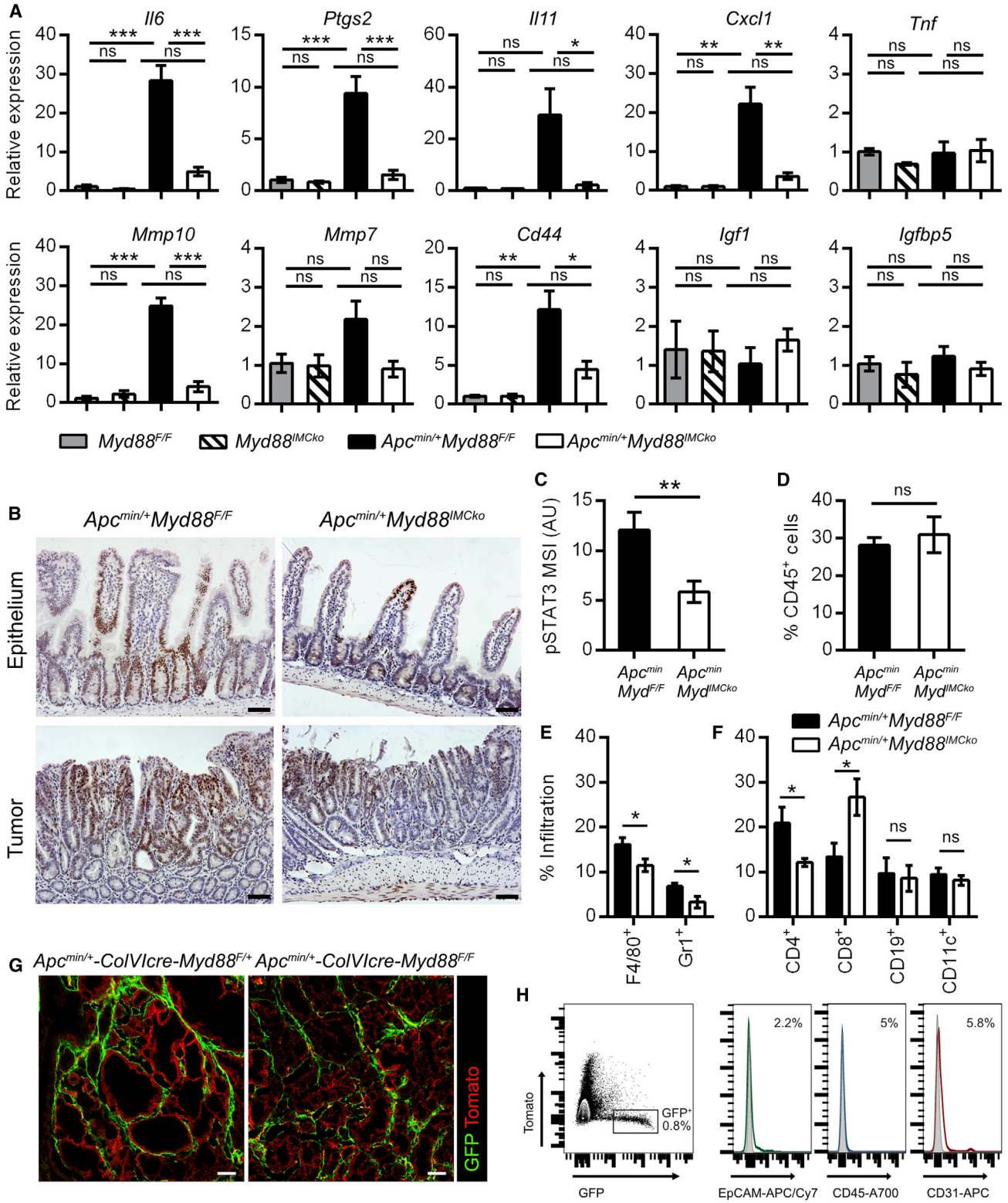

(legend on next page)

phosphatidylinositol 3-kinase (PI3K), and mitogen-activated protein kinases (MAPKs) (Walton et al., 2009). IL-1β mediates the activation of a pro-inflammatory signature in CAFs through the NF-κB pathway and has been implicated in carcinogenesis (Erez et al., 2010). To verify if upstream signaling from TLR4 or IL-1R was responsible for the IMC-specific MyD88-induced effect on intestinal carcinogenesis, we next crossed *Il1r1*$^{F/F}$ (Abdulaal et al., 2016) and *Tlr4*$^{F/F}$ (Sodhi et al., 2012) mice with ColVI-cre mice (Figures S1B and S1C). We found that 4-month-old *Apc*$^{min/+}$-*Il1r1*^{IMCko} mice showed no difference in tumor multiplicity and size (Figures 3C and 3D), indicating that IL-1R signaling in IMCs does not play an important role in spontaneous intestinal carcinogenesis. On the contrary, *Apc*$^{min/+}$-*Tlr4*^{IMCko} showed a significant reduction in both tumor multiplicity and size (Figures 3E–3H). Tumors from these mice also displayed decreased proliferation measured by BrdU staining (Figures 3I and 3J) and decreased phosphorylation of STAT3 (Figures 3I and 3K), as well as reduced expression of inflammatory mediators (Figure 3L). These results are in agreement both with the phenotype observed in *Apc*$^{min/+}$-*Myd88*^{IMCko} and our *in vitro* data, suggesting that upstream signaling from TLR4 drives MyD88 activation in IMCs and concomitant modulation of intestinal tumorigenesis.

We also subjected *Tlr4*^{IMCko} and their controls to the AOM/DSS model of colitis-associated cancer and found no difference in tumorigenesis, in accordance with *Myd88*^{IMCko} mice, indicating that TLR4 signaling in IMCs and/or CAFs is necessary only for the development of sporadic intestinal carcinogenesis (Figure 3M).

An IMC-Specific TLR4/MyD88-Regulated Gene Signature Is Found Also in Human CAFs

To identify the IMC-specific MyD88-dependent gene expression changes, we next performed 3′ RNA sequencing of ColVIcre^{+} wild-type (WT) and MyD88 knockout IMCs before and after treatment with LPS for 6 h. Interestingly, even unstimulated MyD88 knockout cells showed a significantly altered gene expression profile in comparison to the unstimulated control cells (Figure S4A). Gene Ontology (GO) analysis of the mostly downregulated genes in non-induced MyD88 knockout cells revealed differences in pathways related to inflammatory and/or immune response and cell proliferation, indicating an intrinsic defect of these cells in acquiring an innate identity under homeostatic conditions (Figures 4A and 4D). Comparisons with the LPS-stimulated control and MyD88 knockout samples further showed a significant number of MyD88-regulated genes, which either remained unchanged or were altered upon LPS stimulation (Figure 4B; Figures S4B and S4C). GO analysis of these MyD88-regulated genes showed enrichment in inflammatory and/or immune response and regulation of cell proliferation (Figure 4C). Related genes included mainly chemokines (*Cxcl1*, *Cxcl2*, *Cxcl5*, *Ccl2*, *Ccl7*, *Ccl8*, *Ccl11*), cytokines (*Il6*, *Il34*), growth factors (*Fgf7*, *Fgf10*, *Tgfa*, *Ctgf*, *Igf1*, *Igfbp4*), and MMPs (*Mmp3*, *Mmp8*, *Mmp9*, *Mmp10*, *Mmp13*) (Figure 4D). This MyD88-dependent gene signature is in agreement with the deregulated gene expression of the IMC-specific MyD88 knockout tumors and the accompanied reduced proliferation and altered inflammatory infiltration.

To further validate if this expression profile was also present in human CAFs, we next compared this MyD88-regulated gene profile with two datasets that contained comparisons of CAFs versus cancer cells (GEO: GSE39395 and GSE35602) (Calon et al., 2012; Nishida et al., 2012). We found that out of 120 genes, 68 and 65 were preferentially expressed in CAFs in each dataset, respectively, while 53 were in common between the two lists (Figures 4E and 4F). These included cytokines (*IL6*), chemokines (*CCL2*, *CCL8*, *CCL11*), growth factors (*FGF7*, *CTGF*, *IGF1*), and MMPs (*MMP3*, *MMP10*, *MMP13*) (Figure 4F), suggesting that a similar TLR4/MyD88-regulated gene signature exists also in human CAFs.

DISCUSSION

MyD88 is known to have a tumor-promoting role in spontaneous intestinal cancer (Rakoff-Nahoum and Medzhitov, 2007). Here we show, through its IMC-specific deletion, that it is MyD88 in IMCs that is responsible for this function, in agreement with previous bone marrow transfer studies, indicating a predominant role of MyD88 in the non-hematopoietic compartment (Lee et al., 2010). It should be noted that the phenotypic differences between the IMC-specific and the published complete MyD88 knockout mice also suggest a possible contribution of MyD88 in other non-hematopoietic cell types, including other mesenchymal cell populations.

In agreement with these data, IMC-specific TLR4, but not ILR1, ablation also ameliorates intestinal tumorigenesis,

Figure 2. Tumors from Mice with Deletion of MyD88 in IMCs Show Differential Gene Expression, Reduced STAT3 Activation, and Altered Inflammatory Cell Infiltration

(A) Gene expression analysis in the small intestine of *Myd88*$^{F/F}$ and *Myd88*^{IMCko} mice (n = 3) and in tumors from *Apc*$^{min/+}$*Myd88*$^{F/F}$ and *Apc*$^{min/+}$*Myd88*^{IMCko} mice (n = 6). *Hprt* was used for normalization.

(B) Representative immunohistochemical staining for pSTAT3 in the normal small intestine and tumors of *Apc*$^{min/+}$*Myd88*$^{F/F}$ and *Apc*$^{min/+}$*Myd88*^{IMCko} mice (n = 5 mice per genotype).

(C) Quantification of pSTAT3 staining in tumors from *Apc*$^{min/+}$*Myd88*$^{F/F}$ and *Apc*$^{min/+}$*Myd88*^{IMCko} mice (n = 12–14 tumors from 5 mice per genotype).

(D–F) Infiltration of CD45^{+} cells (D), CD11b^{+}F4/80^{+} macrophages and CD11b^{+}Gr1^{+} neutrophils (E), and CD4^{+} T cells, CD8^{+} T cells, CD19^{+} B cells, and CD11c^{+} dendritic cells (F) in tumors from 4- to 5-month-old *Apc*$^{min/+}$*Myd88*$^{F/F}$ and *Apc*$^{min/+}$*Myd88*^{IMCko} mice (n = 4–7), quantified by FACS analysis (from two independent experiments).

(G) Representative confocal images from tumors of *Apc*$^{min/+}$-ColVIcre-*Myd88*$^{F/+}$-mTmG and *Apc*$^{min/+}$-ColVIcre-*Myd88*$^{F/F}$-mTmG mice (n = 3). Scale bars represent 50 μm.

(H) FACS analysis of tumors from *Apc*$^{min/+}$-ColVIcre-mTmG mice, stained with markers for epithelial (EpCAM), immune (CD45), and endothelial (CD31) cells (n = 3 mice). Unstained controls are presented as gray histograms.

Data represent mean ± SEM. *p < 0.05, **p < 0.01, ***p < 0.001, ns = not significant. See also Figure S3.

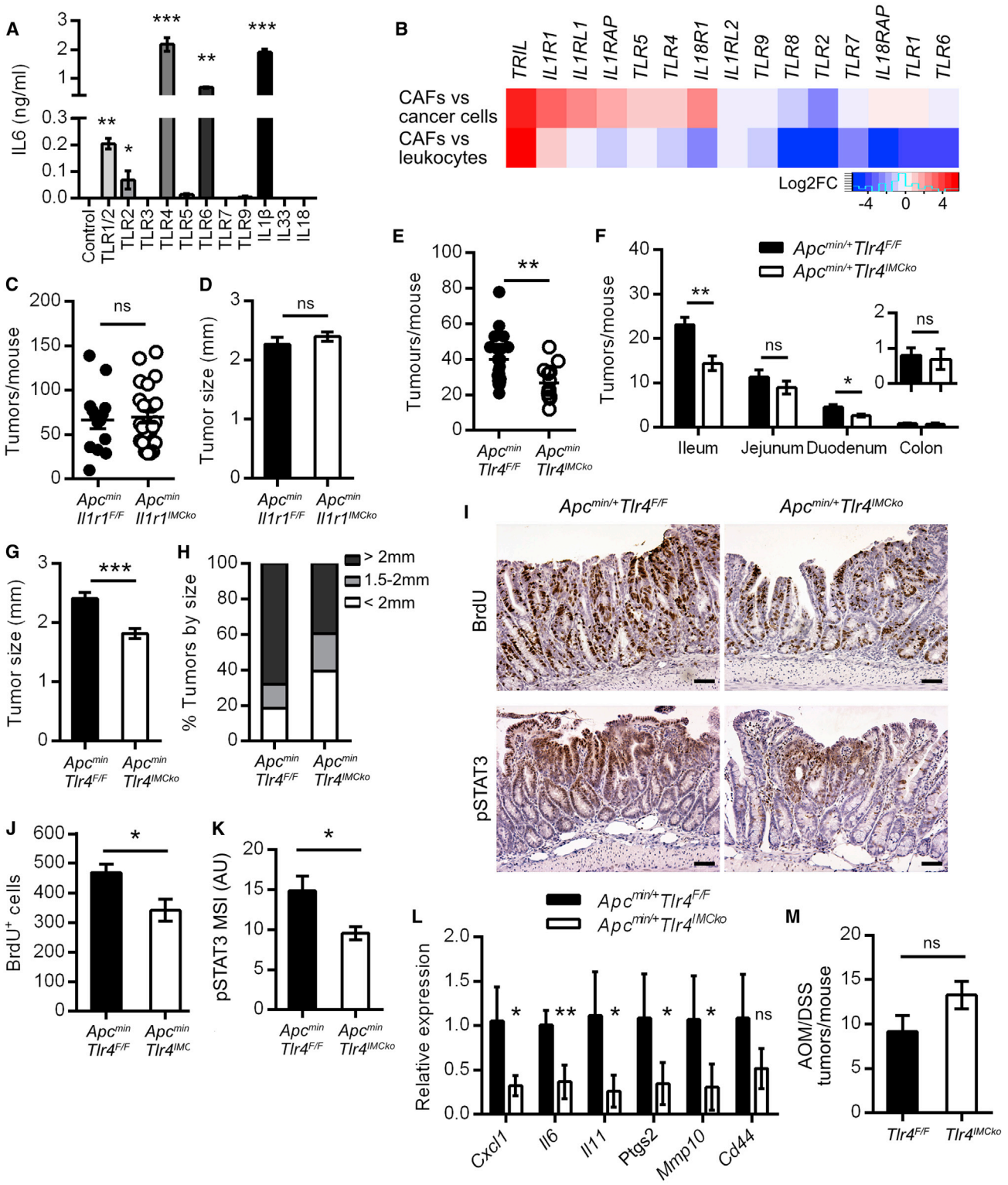

Figure 3. Deletion of TLR4 in IMCs Reduces Tumorigenesis in the *Apc*$^{min/+}$ Model of Sporadic Intestinal Cancer

(A) IL-6 quantification by ELISA in the supernatants of IMCs stimulated for 24 h with TLRs and interleukins, as described in STAR Methods. One representative of three independent experiments performed in triplicates is presented.

(B) Heatmap of the differential expression of the indicated genes in CAFs versus cancer cells and leukocytes from the dataset GEO: GSE39395. Log2 fold-change of genes is shown. Red denotes high expression values, and blue denotes low expression values.

(legend continued on next page)

indicating that microbial sensing by these cells may be a pathogenic mechanism in the development of the disease. Although many ligands for TLR4 have been described and may be (co) responsible for the TLR4 effects described here, a potential source for TLR4 stimulation could be LPS from bacteria that are detected close to neoplastic lesions and within tumors in the intestine (Grivennikov et al., 2012). Recently, a specific species, *Fusobacterium nucleatum*, which is a Gram-negative bacterium, has been found in tumors from human patients and in tumors from $Apc^{min/+}$ mice fed with this strain but not in normal mucosa (Kostic et al., 2013; Yang et al., 2017). Importantly, infection of $Apc^{min/+}$ with this bacterial strain led to increased tumorigenesis, associated with increased proliferation, infiltration of $CD11b^{+}F4/80^{+}$ and $CD11b^{+}Gr1^{+}$ immune cells, and expression of inflammatory genes, such as *Il6*, *Ptgs2*, and *Mmp3* (Kostic et al., 2013). These data indicate that microbes can be found in intestinal tumors and are causally linked to cancer progression. Our study therefore offers a direct mechanistic link between intratumoral bacterial sensing and innate activation of IMCs and/or CAFs that together contribute strongly to tumor progression.

Our *ex vivo* data indicated that the mechanism downstream of innate sensing in IMCs includes the production of effector molecules, which in turn affect both cancer cell proliferation and the immune microenvironment, mainly during the progression rather than the initiation stage of spontaneous tumorigenesis. Among them, IL-6/IL-11 and downstream-regulated STAT3 signaling is an important pro-tumorigenic mechanism (Bollrath et al., 2009; Schmidt et al., 2018). Interestingly, we have recently published that inhibitor of nuclear factor κB subunit β (IKKβ) deletion in IMCs leads to reduced inflammation and carcinogenesis in the AOM/DSS model of colitis-associated cancer, which is mediated by the production of IL-6 and downstream phosphor-STAT3 (pSTAT3) phosphorylation, while it does not affect carcinogenesis in the sporadic $Apc^{1638N/+}$ or AOM model (Koliaraki et al., 2015). The $Myd88^{IMCko}$ mice and $Tlr4^{IMCko}$ mice show an opposite phenotype, affecting the number and size of tumors in spontaneous, but not in colitis-associated, cancer. These results suggest that production of IL-6 and other inflammatory cytokines and/or chemokines is mediated in IMCs through the NF-κB pathway, which can be activated, but not exclusively, by Myd88-dependent signals in the early stages of colitis associated cancer (CAC). In spontaneous intestinal cancer, this cytokine and/or chemokine production is induced largely by the TLR4/MyD88 pathway, and it is notably not dependent on NF-κB, indicating heterogeneous signaling in the context of IMC and/or CAF innate activation, which is probably regulated by the distinct microenvironment of the tumors. It should be noted that in the $Apc^{min/+}$ model, the colon tumor number, although very low, was also not affected, implying that potential site-specific differences, such as the mesenchymal population targeted by the ColVI-cre mouse, could also play a role in the absence of a phenotype.

Besides IL-6, a variety of other effector molecules, such as growth factors, chemokines, and MMPs, are also regulated by the TLR4/MyD88 pathway in IMCs. A pro-inflammatory gene expression profile has been found also in other types of cancer (Erez et al., 2010), and the role of specific cytokines and chemokines in cancer promotion is now well established (Terzic et al., 2010). Interestingly, we have found that many of these are also found enriched in CAFs from human colorectal cancer, suggesting a potential role for innate responses also in human tumors and their possible utility as prognostic markers. For example, MMP3 and CXCL1 have already been suggested as potent stromal protein markers of dysplasia-to-carcinoma transition in sporadic colorectal cancer (Sipos et al., 2014).

In conclusion, our results reveal the cellular specificity of MyD88's function in spontaneous intestinal carcinogenesis and provide direct evidence for a pathophysiological significant innate immune function of IMCs and CAFs in cancer. This suggests that these cells could directly respond to the microbiota and that this response is crucial for tumor growth, providing a conceptual advance on the regulation, functions, and potential therapeutic targeting of CAFs, including recent efforts to enhance immune targeting of cancer.

STAR★METHODS

Detailed methods are provided in the online version of this paper and include the following:

- KEY RESOURCES TABLE
- CONTACT OR REAGENT AND RESOURCE SHARING
- EXPERIMENTAL MODEL AND SUBJECT DETAILS
  - Mice
  - Model Systems and Permissions
  - Isolation and Induction of Primary IMCs
- METHOD DETAILS
  - Induction of Colitis-associated Cancer
  - Histology and Immunohistochemistry
  - FACS analysis and Cell Sorting

(C and D) Total number (C) and size (D) of tumors per mouse in 4-month-old $Apc^{min/+}Il1r1^{IMCko}$ mice (n = 14) and their littermate controls (n = 24).
(E and F) Total number of tumors per mouse (E) and number of tumors per intestinal part (F) in 4-month-old $Apc^{min/+}Tlr4^{IMCko}$ mice (n = 13) and their littermate controls (n = 20). The insert shows the number of tumors in the colon.
(G and H) Mean tumor size (G) and distribution of tumors (H) per size in the two genotypes.
(I) Representative BrdU and pSTAT3 staining in small intestinal tumors of $Apc^{min/+}Tlr4^{IMCko}$ mice and their littermate controls. Scale bar = 50 μm.
(J) Quantification of the number of $BrdU^{+}$ cells per tumor (n = 6 mice per genotype).
(K) Mean signal intensity (MSI) of pSTAT3 (n = 12–14 tumors from 4 mice per genotype).
(L) Gene expression analysis in tumors from $Apc^{min/+}Tlr4^{F/F}$ and $Apc^{min/+}Tlr4^{IMCko}$ mice (n = 6). *Hprt* was used for normalization.
(M) Number of tumors per mouse in $Tlr4^{IMCko}$ mice (n = 8) and their littermate controls (n = 8) at the end of the AOM/DSS protocol (one representative experiment of three performed).
Data represent mean ± SEM. *p < 0.05, **p < 0.01, ***p < 0.001, ns = not significant. See also Figure S1.

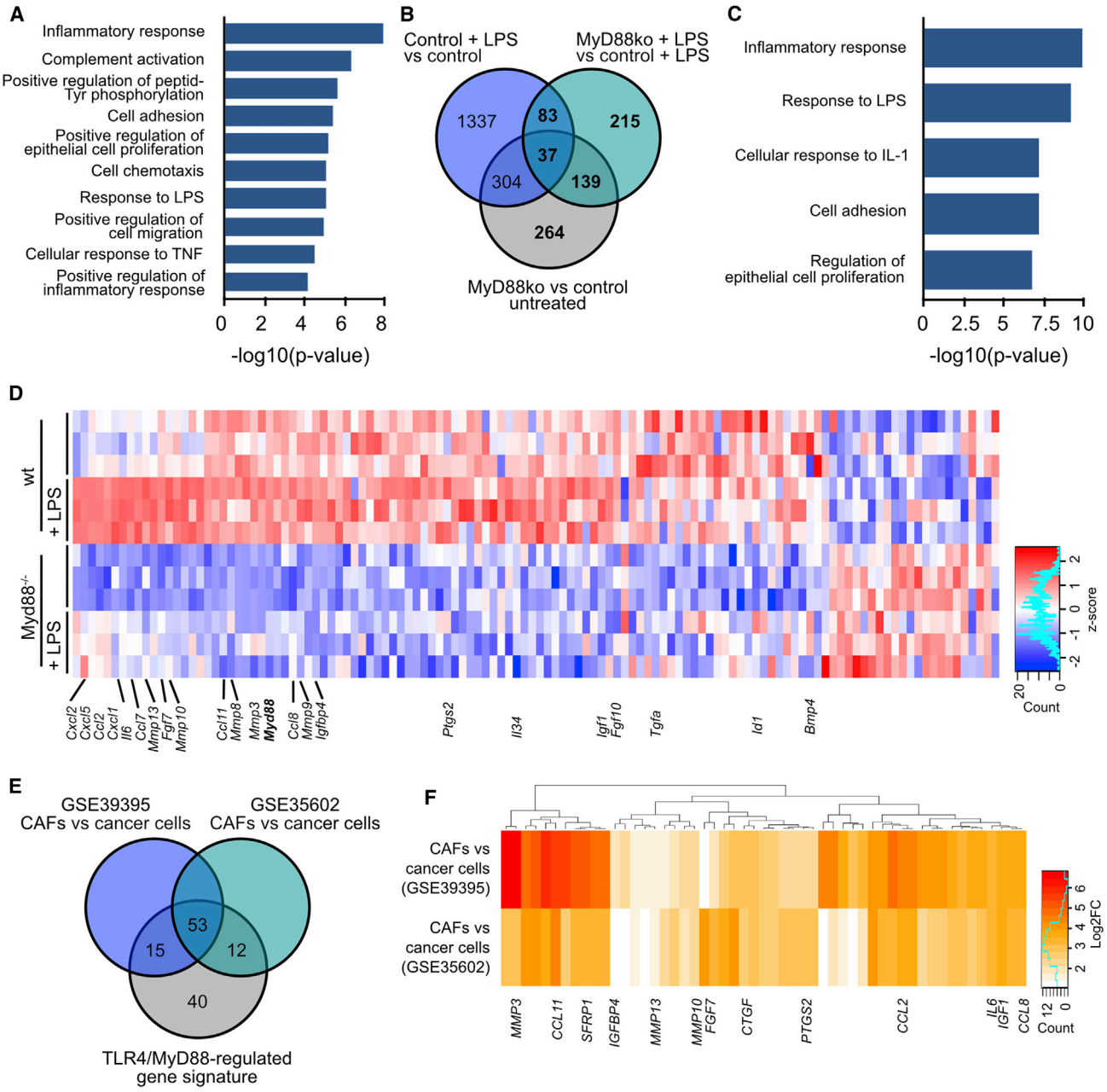

Figure 4. TLR4/MyD88 Signaling Induces a Pro-Tumorigenic Gene Signature in IMCs

(A) Gene Ontology (GO) terms enriched in differentially expressed genes between untreated control and MyD88 knockout IMCs.

(B) Venn diagram showing the number of overlapping differentially regulated genes between untreated and LPS-treated control and MyD88 knockout IMCs.

(C) GO terms enriched in MyD88-regulated genes indicated as bold in (B).

(D) Heatmap of differentially expressed genes between control and LPS-induced WT and MyD88 knockout IMCs that belong to the GO terms shown in (C). Log2 transformed normalized read counts of genes are shown. Read counts are scaled per column. Red denotes high expression values, and blue denotes low expression values.

(E and F) Venn diagram showing the number of overlapping genes (E) and heatmap of their expression between the IMC-specific MyD88-regulated gene signature and genes overexpressed in CAFs versus cancer cells from the datasets GEO: GSE39395 and GSE35602 (F). Log2 fold-change of genes is shown.

See also Figure S4.

- ELISA
  - RNA Isolation and qRT-PCR
  - 3′ RNA-Seq sequencing
- QUANTIFICATION AND STATISTICAL ANALYSIS
  - Analysis of RNaseq data
  - Datasets and Statistical analysis
- DATA AND SOFTWARE AVAILABILITY

SUPPLEMENTAL INFORMATION

Supplemental Information includes four figures and one table and can be found with this article online at https://doi.org/10.1016/j.celrep.2018.12.072.

ACKNOWLEDGMENTS

We thank Michalis Meletiou, Anna Katevaini, and Spiros Lalos for technical assistance in mouse genotyping and histology. We thank Sofia Grammenoudi for assistance in flow cytometry. We thank the Genomics Facility of BSRC "Alexander Fleming," specifically Vaggelis Harokopos for performing RNA sequencing and Martin Reczko for initial bioinformatics analyses. We also thank the InfrafrontierGR infrastructure (co-funded by the European Regional Development Fund and Greek NSRF 2007-2013 to G.K.) for providing mouse hosting and phenotyping facilities. This work was supported by a grant from the Stavros Niarchos Foundation to the BSRC "Alexander Fleming" as part of the Foundation's initiative to support the Greek research center ecosystem and the FP7 Advanced ERC Grant MCs-inTEST (grant 340217) to G.K.

AUTHOR CONTRIBUTIONS

Conceptualization, V.K. and G.K.; Investigation, V.K., N.C., A.H., and A.P.; Formal Analysis and Visualization, V.K., N.C., A.H., and C.T.; Data Curation, C.T.; Writing – Original Draft, V.K; Writing – Review & Editing, M.P. and G.K; Resources, M.P., D.J.H., A.W., and W.M.; Funding Acquisition, G.K.; Supervision, V.K. and G.K.

DECLARATION OF INTERESTS

The authors declare no competing interests.

Received: August 31, 2018
Revised: November 5, 2018
Accepted: December 17, 2018
Published: January 15, 2019

REFERENCES

Abdulaal, W.H., Walker, C.R., Costello, R., Redondo-Castro, E., Mufazalov, I.A., Papaemmanouil, A., Rothwell, N.J., Allan, S.M., Waisman, A., Pinteaux, E., and Müller, W. (2016). Characterization of a conditional interleukin-1 receptor 1 mouse mutant using the Cre/LoxP system. Eur. J. Immunol. *46*, 912–918.

Armaka, M., Apostolaki, M., Jacques, P., Kontoyiannis, D.L., Elewaut, D., and Kollias, G. (2008). Mesenchymal cell targeting by TNF as a common pathogenic principle in chronic inflammatory joint and intestinal diseases. J. Exp. Med. *205*, 331–337.

Bollrath, J., Phesse, T.J., von Burstin, V.A., Putoczki, T., Bennecke, M., Bateman, T., Nebelsiek, T., Lundgren-May, T., Canli, O., Schwitalla, S., et al. (2009). gp130-mediated Stat3 activation in enterocytes regulates cell survival and cell-cycle progression during colitis-associated tumorigenesis. Cancer Cell *15*, 91–102.

Calon, A., Espinet, E., Palomo-Ponce, S., Tauriello, D.V., Iglesias, M., Céspedes, M.V., Sevillano, M., Nadal, C., Jung, P., Zhang, X.H., et al. (2012). Dependency of colorectal cancer on a TGF-β-driven program in stromal cells for metastasis initiation. Cancer Cell *22*, 571–584.

Ding, M., Bruick, R.K., and Yu, Y. (2016). Secreted IGFBP5 mediates mTORC1-dependent feedback inhibition of IGF-1 signalling. Nat. Cell Biol. *18*, 319–327.

Dove, W.F., Clipson, L., Gould, K.A., Luongo, C., Marshall, D.J., Moser, A.R., Newton, M.A., and Jacoby, R.F. (1997). Intestinal neoplasia in the ApcMin mouse: independence from the microbial and natural killer (beige locus) status. Cancer Res. *57*, 812–814.

Erez, N., Truitt, M., Olson, P., Arron, S.T., and Hanahan, D. (2010). Cancer-Associated Fibroblasts Are Activated in Incipient Neoplasia to Orchestrate Tumor-Promoting Inflammation in an NF-kappaB-Dependent Manner. Cancer Cell *17*, 135–147.

Grivennikov, S.I., Wang, K., Mucida, D., Stewart, C.A., Schnabl, B., Jauch, D., Taniguchi, K., Yu, G.Y., Osterreicher, C.H., Hung, K.E., et al. (2012). Adenoma-linked barrier defects and microbial products drive IL-23/IL-17-mediated tumour growth. Nature *491*, 254–258.

Hanahan, D., and Coussens, L.M. (2012). Accessories to the crime: functions of cells recruited to the tumor microenvironment. Cancer Cell *21*, 309–322.

Heberle, H., Meirelles, G.V., da Silva, F.R., Telles, G.P., and Minghim, R. (2015). InteractiVenn: a web-based tool for the analysis of sets through Venn diagrams. BMC Bioinformatics *16*, 169.

Henriques, A., Koliaraki, V., and Kollias, G. (2018). Mesenchymal MAPKAPK2/HSP27 drives intestinal carcinogenesis. Proc. Natl. Acad. Sci. USA *115*, E5546–E5555.

Huang, D.W., Sherman, B.T., and Lempicki, R.A. (2009a). Bioinformatics enrichment tools: paths toward the comprehensive functional analysis of large gene lists. Nucleic Acids Res. *37*, 1–13.

Huang, D.W., Sherman, B.T., and Lempicki, R.A. (2009b). Systematic and integrative analysis of large gene lists using DAVID bioinformatics resources. Nat. Protoc. *4*, 44–57.

Koliaraki, V., and Kollias, G. (2016). Isolation of intestinal mesenchymal cells from adult mice. Bio-protocol *6*, e1940.

Koliaraki, V., Roulis, M., and Kollias, G. (2012). Tpl2 regulates intestinal myofibroblast HGF release to suppress colitis-associated tumorigenesis. J. Clin. Invest. *122*, 4231–4242.

Koliaraki, V., Pasparakis, M., and Kollias, G. (2015). IKKβ in intestinal mesenchymal cells promotes initiation of colitis-associated cancer. J. Exp. Med. *212*, 2235–2251.

Koliaraki, V., Pallangyo, C.K., Greten, F.R., and Kollias, G. (2017). Mesenchymal Cells in Colon Cancer. Gastroenterology *152*, 964–979.

Kostic, A.D., Chun, E., Robertson, L., Glickman, J.N., Gallini, C.A., Michaud, M., Clancy, T.E., Chung, D.C., Lochhead, P., Hold, G.L., et al. (2013). Fusobacterium nucleatum potentiates intestinal tumorigenesis and modulates the tumor-immune microenvironment. Cell Host Microbe *14*, 207–215.

Lee, S.H., Hu, L.L., Gonzalez-Navajas, J., Seo, G.S., Shen, C., Brick, J., Herdman, S., Varki, N., Corr, M., Lee, J., and Raz, E. (2010). ERK activation drives intestinal tumorigenesis in Apc(min/+) mice. Nat. Med. *16*, 665–670.

Li, Y., Kundu, P., Seow, S.W., de Matos, C.T., Aronsson, L., Chin, K.C., Kärre, K., Pettersson, S., and Greicius, G. (2012). Gut microbiota accelerate tumor growth via c-jun and STAT3 phosphorylation in APCMin/+ mice. Carcinogenesis *33*, 1231–1238.

Moulos, P., and Hatzis, P. (2015). Systematic integration of RNA-Seq statistical algorithms for accurate detection of differential gene expression patterns. Nucleic Acids Res. *43*, e25.

Muzumdar, M.D., Tasic, B., Miyamichi, K., Li, L., and Luo, L. (2007). A global double-fluorescent Cre reporter mouse. Genesis *45*, 593–605.

Nishida, N., Nagahara, M., Sato, T., Mimori, K., Sudo, T., Tanaka, F., Shibata, K., Ishii, H., Sugihara, K., Doki, Y., and Mori, M. (2012). Microarray analysis of colorectal cancer stromal tissue reveals upregulation of two oncogenic miRNA clusters. Clin. Cancer Res. *18*, 3054–3070.

Powell, D.W., Pinchuk, I.V., Saada, J.I., Chen, X., and Mifflin, R.C. (2011). Mesenchymal cells of the intestinal lamina propria. Annu. Rev. Physiol. *73*, 213–237.

R Core Team (2017). R: A Language and Environment for Statistical Computing (R Foundation for Statistical Computing). https://www.R-project.org/.

Rakoff-Nahoum, S., and Medzhitov, R. (2007). Regulation of spontaneous intestinal tumorigenesis through the adaptor protein MyD88. Science *317*, 124–127.

Roulis, M., Nikolaou, C., Kotsaki, E., Kaffe, E., Karagianni, N., Koliaraki, V., Salpea, K., Ragoussis, J., Aidinis, V., Martini, E., et al. (2014). Intestinal myofibroblast-specific Tpl2-Cox-2-PGE2 pathway links innate sensing to epithelial homeostasis. Proc. Natl. Acad. Sci. USA *111*, E4658–E4667.

Salcedo, R., Worschech, A., Cardone, M., Jones, Y., Gyulai, Z., Dai, R.M., Wang, E., Ma, W., Haines, D., O'hUigin, C., et al. (2010). MyD88-mediated signaling prevents development of adenocarcinomas of the colon: role of interleukin 18. J. Exp. Med. *207*, 1625–1636.

Salcedo, R., Cataisson, C., Hasan, U., Yuspa, S.H., and Trinchieri, G. (2013). MyD88 and its divergent toll in carcinogenesis. Trends Immunol. *34*, 379–389.

Schmidt, S., Schumacher, N., Schwarz, J., Tangermann, S., Kenner, L., Schlederer, M., Sibilia, M., Linder, M., Altendorf-Hofmann, A., Knösel, T., et al. (2018). ADAM17 is required for EGF-R-induced intestinal tumors via IL-6 trans-signaling. J. Exp. Med. *215*, 1205–1225.

Sipos, F., Germann, T.M., Wichmann, B., Galamb, O., Spisák, S., Krenács, T., Tulassay, Z., Molnár, B., and Műzes, G. (2014). MMP3 and CXCL1 are potent stromal protein markers of dysplasia-carcinoma transition in sporadic colorectal cancer. Eur. J. Cancer Prev. *23*, 336–343.

Sodhi, C.P., Neal, M.D., Siggers, R., Sho, S., Ma, C., Branca, M.F., Prindle, T., Jr., Russo, A.M., Afrazi, A., Good, M., et al. (2012). Intestinal epithelial Toll-like receptor 4 regulates goblet cell development and is required for necrotizing enterocolitis in mice. Gastroenterology *143*, 708–718.e5.

Song, X., Gao, H., Lin, Y., Yao, Y., Zhu, S., Wang, J., Liu, Y., Yao, X., Meng, G., Shen, N., et al. (2014). Alterations in the microbiota drive interleukin-17C production from intestinal epithelial cells to promote tumorigenesis. Immunity *40*, 140–152.

Terzic, J., Grivennikov, S., Karin, E., and Karin, M. (2010). Inflammation and colon cancer. Gastroenterology *138*, 2101–2114.e5.

Tomasetti, C., and Vogelstein, B. (2015). Cancer etiology. Variation in cancer risk among tissues can be explained by the number of stem cell divisions. Science *347*, 78–81.

Vlantis, K., Polykratis, A., Welz, P.S., van Loo, G., Pasparakis, M., and Wullaert, A. (2016). TLR-independent anti-inflammatory function of intestinal epithelial TRAF6 signalling prevents DSS-induced colitis in mice. Gut *65*, 935–943.

Walton, K.L., Holt, L., and Sartor, R.B. (2009). Lipopolysaccharide activates innate immune responses in murine intestinal myofibroblasts through multiple signaling pathways. Am. J. Physiol. Gastrointest. Liver Physiol. *296*, G601–G611.

Warnes, G.R., Bolker, B., Bonebakker, L., Gentleman, R., Liaw, W.H.A., Lumley, T., Maechler, M., Magnusson, A., Moeller, S., Schwartz, M., et al. (2016). gplots: Various R programming tools for plotting data. Package version 3.0.1. https://cran.r-project.org/web/packages/gplots/index.html.

Wickham, H. (2016). ggplot2: Elegant Graphics for Data Analysis (Springer-Verlag).

Wirtz, S., Popp, V., Kindermann, M., Gerlach, K., Weigmann, B., Fichtner-Feigl, S., and Neurath, M.F. (2017). Chemically induced mouse models of acute and chronic intestinal inflammation. Nat. Protoc. *12*, 1295–1309.

Yang, Y., Weng, W., Peng, J., Hong, L., Yang, L., Toiyama, Y., Gao, R., Liu, M., Yin, M., Pan, C., et al. (2017). Fusobacterium nucleatum Increases Proliferation of Colorectal Cancer Cells and Tumor Development in Mice by Activating Toll-Like Receptor 4 Signaling to Nuclear Factor-kappaB, and Up-regulating Expression of MicroRNA-21. Gastroenterology *152*, 851–866.e24.

STAR★METHODS

KEY RESOURCES TABLE

REAGENT or RESOURCE	SOURCE	IDENTIFIER
Antibodies		
Rabbit anti-Phospho-STAT3 (Tyr705)	Cell Signaling	Cat#9131; RRID: AB_331586
Purified Rat anti-mouse CD16/32	Biolegend	Cat#101302; RRID: AB_312801
FITC-conjugated Rat anti-mouse CD11b (clone M1/70)	eBioscience	Cat#11-0112-85; RRID: AB_464936
APC/Cy7-conjugated Rat anti-mouse CD45 (clone 30-F11)	Biolegend	Cat#103116; RRID: AB_312981
A700-conjugated Rat anti-mouse CD45 (clone 30-F11)	Biolegend	Cat#103128; RRID: AB_493715
PE/Cy7-conjugated Armenian Hamster anti-mouse CD11c (clone N418)	Biolegend	Cat#117318; RRID: AB_493568
A700-conjugated Rat anti-mouse CD19 (clone eBio1D3 (1D3))	eBioscience	Cat#56-0193-80; RRID: AB_837082
A700-conjugated Rat anti-mouse CD4 (RM4-5)	eBioscience	Cat#56-0042-82; RRID: AB_494000
APC-conjugated Rat anti-mouse CD8a (clone 53-6.7)	Biolegend	Cat#100712; RRID: AB_312751
A647-conjugated Rat anti-mouse Gr-1 (clone RB6-8C5)	Biolegend	Cat#108418; RRID: AB_389331
PE-conjugated Rat anti-mouse F4/80 (clone BM8)	eBioscience	Cat#12-4801-82; RRID: AB_465923
Streptavidin-conjugated A750	Life Technologies	Cat#S21384
Biotinylated Goat Anti-Rabbit IgG	Vector Laboratories	Cat#BA-1000; RRID: AB_2313606
Chemicals, Peptides, and Recombinant Proteins		
Collagenase IV	Sigma-Aldrich	C5138
Collagenase XI	Sigma-Aldrich	C7657
Deoxyribonuclease I from bovine pancreas (DNase I)	Sigma-Aldrich	DN25
Dispase II, powder	Roche	25766800/04942078001
DMEM	Biochrom	F0455
Fetal Bovine Serum (FBS)	Biosera	FB-1001/500
Antibiotic-antimycotic solution	GIBCO	15240-062
L-Glutamine	GIBCO	25030-024
Nonessential amino acids (MEM NEAA)	GIBCO	11140-035
Penicillin and streptomycin	GIBCO	15140-122
Amphotericin B	Sigma-Aldrich	A2942
Propidium Iodide Solution	Sigma-Aldrich	255535-16-4
BrdU, powder	Roche	10 280 879 001
Vectastain ABC	Vector Laboratories	PK-6100
ImmPACT DAB Peroxidase (HRP) Substrate	Vector Laboratories	SK-4105
MMLV Reverse Transcriptase	Promega	M1701
Platinum SYBR-Green qPCR SuperMix	Invitrogen	11733046
Oligo-dT primers	New England BioLabs	S1316S
Azoxymethane (AOM)	Sigma-Aldrich	A5486
Dextran Sodium Sulfate (DSS)	MP Biomedicals	M9147
LPS from *E. coli*	Sigma-Aldrich	L2630
Recombinant Murine IL-1β	Peprotech	211-11B
Recombinant Mouse IL-18	MBL	B002-5
Recombinant Mouse IL-33	R&D Systems	3626-ML
Critical Commercial Assays		
RNeasy Mini Kit	QIAGEN	74104
RNeasy Micro Kit	QIAGEN	74004
Mouse IL-6 Duo-Set ELISA	R&D Systems	DY4046

(*Continued on next page*)

Continued

REAGENT or RESOURCE	SOURCE	IDENTIFIER
BrdU Proliferation kit	BD Biosciences	550803
DeadEnd Fluorometric Tunel assay	Promega	G3250
Mouse TLR1-9 Agonist kit	Invivogen	tlrl-kit1mw
Agilent RNA 6000 Nano kit	Agilent Technologies	5067-1511
QuantSeq 3′ mRNA-Seq Library Prep Kit for Ion Torrent	Lexogen	012
DNA High Sensitivity Kit	Agilent Technologies	5067-4626
Ion PI™ IC 200 Kit	ThermoFisher Scientific	4488377
Ion PI™ Sequencing 200 V3 Kit	ThermoFisher Scientific	4488315
Ion Proton PI™ V2 chips	ThermoFisher Scientific	4482321
Deposited Data		
Normalized data	Calon et al., 2012	GEO: GSE39395
Normalized data	Nishida et al., 2012	GEO: GSE35602
Raw and analyzed data	This study	GEO: GSE119341
Experimental Models: Organisms/Strains		
Mouse: C57BL/6J-*ApcMin*/J	Jackson Laboratory	https://www.jax.org/strain/002020
Mouse: B6.129(Cg)-*Gt(ROSA)26Sor*$^{tm4(ACTB-tdTomato,-EGFP)Luo}$/J	Jackson Laboratory	https://www.jax.org/strain/007676
Mouse: *Tg*(CollagenVI-Cre)	Kollias Laboratory	Armaka et al., 2008
Mouse: *Myd88*$^{f/f}$	Pasparakis Laboratory	Vlantis et al., 2016
Mouse: *Tlr4*$^{f/f}$	Hackam Laboratory	Sodhi et al., 2012
Mouse: *Il1r1*$^{f/f}$	Muller Laboratory	Abdulaal et al., 2016
Oligonucleotides		
See Table S1 for primer sequences	This study; Salcedo et al., 2010; Ding et al., 2016	N/A
Software and Algorithms		
ImageJ	National Center for Microscopy and Imaging Research	RRID: SCR_003070
GraphPad Prism	GraphPad	RRID: SCR_002798
Leica Application Suite X	Leica Microsystems	RRID: SCR_013673
Opticon Monitor	Bio-Rad	RRID: SCR_014241
FACSDiva	BD Biosciences	RRID: SCR_001456
FlowJo	Tree Star Inc	RRID: SCR_008520
Geo2R function	NCBI	N/A
InteractiveVenn	Heberle et al., 2015; http://www.interactivenn.net	N/A
Functional Annotation tool from DAVID for Gene Ontologies	Huang et al., 2009a, 2009b; https://david.ncifcrf.gov/	N/A

CONTACT OR REAGENT AND RESOURCE SHARING

Further information and requests for resources and reagents should be directed to and will be fulfilled by the Lead Contact, George Kollias (kollias@fleming.gr).

EXPERIMENTAL MODEL AND SUBJECT DETAILS

Mice

Myd88$^{F/F}$, *Tlr4*$^{F/F}$, *Il1r1*$^{F/F}$ and ColVI-cre mice have been previously described (Abdulaal et al., 2016; Armaka et al., 2008; Sodhi et al., 2012; Vlantis et al., 2016). *Rosa*^{mTmG} and *Apc*$^{min/+}$ mice were purchased from the Jackson Laboratory (Dove et al., 1997; Muzumdar et al., 2007). Both male and female mice were used at the ages of 2-4 months. All mice were maintained on a C57/Bl6 background and

experiments were performed using littermate and co-housed (according to gender) control and experimental mice. Experiments were performed in the animal facilities of Biomedical Sciences Research Center (BSRC) "Alexander Fleming" under specific pathogen–free conditions. Mice were euthanized by CO_2 asphyxiation.

Model Systems and Permissions

All animal studies were approved by the Institutional Committee of Protocol Evaluation in conjunction with the Veterinary Service Management of the Hellenic Republic Prefecture of Attika according to all current European and national legislation and performed in accordance with the guidance of the Institutional Animal Care and Use Committee of BSRC "Alexander Fleming."

Isolation and Induction of Primary IMCs

Isolation and culture of primary intestinal mesenchymal cells was performed as previously described (Koliaraki and Kollias, 2016). In more detail, the small intestine was removed, flushed with ice-cold HBSS (GIBCO), containing antibiotic-antimycotic solution (GIBCO), opened longitudinally and cut into 1 cm pieces. Fat, adherent connective tissue and Peyer's patches were removed. Intestinal pieces were incubated with pre-warmed 5mM EDTA (Acros Organics) and 1 mM DTT (Sigma) in HBSS for 20 minutes at 37°C with horizontal shaking to remove the epithelial layer, washed extensively and then digested using 300u/ml Collagenase XI (Sigma) and 0.1mg/ml Dispase II (Roche) for approximately 40 minutes at 37°C. The resulting supernatant was passed through a 70 μm strainer and single cells were pelleted by centrifugation at 300*g* for 5 minutes and plated in DMEM (Biochrom), supplemented with 10% FBS, (Biochrom), 2 mM L-glutamine (GIBCO) 1% nonessential amino acids (GIBCO), 100 U/ml penicillin and 100 μg/ml streptomycin (GIBCO), and 1 μg/ml amphotericin B (Sigma-Aldrich) until confluent. Cells were used at passages 3-4. For induction assays, cells were plated, serum starved overnight, and stimulated with 2 μg/ml LPS from *E. coli* (Sigma), 10ng/ml IL1β (Peprotech), IL33 (MBL), IL18 (R&D systems) and the mouse TLR1-9 Agonist kit (Invivogen). The quantities used for the TLR agonists were 100ng/ml Pam3CSK4 (TLR1/2), $2x10^7$/ml HKLM cells (TLR2), 10 μg/ml poly(I:C) (TLR3), 100ng/ml FLA-ST (TLR5), 100ng/ml FSL1 (TLR6/2), 1 μg/ml ssRNA/Lyovec (TLR7) and 1μM ODN1826 (TLR9).

METHOD DETAILS

Induction of Colitis-associated Cancer

Induction of colitis-associated cancer was performed as previously described (Koliaraki et al., 2015; Wirtz et al., 2017). In more detail, littermate and co-housed 6-8 weeks old male and female mice were injected with 10mg/Kg AOM (Sigma), followed by three cycles of 2.5% DSS (MP Biomedicals, colitis grade, MW: 36–50 kDa) administration in the drinking water. Each cycle lasted 5 days and was followed by 16 days of regular drinking water. Body weights and animal well-being were monitored throughout the study. The mice were euthanized 10 days after the end of the last DSS cycle (Day 60), colon was removed and macroscopically visible tumors were counted.

Histology and Immunohistochemistry

Mice were sacrificed, and the intestine was resected, opened longitudinally, and tumors were counted. Tissues were either fixed overnight in 10% formalin and embedded in paraffin or fixed in 4% Paraformaldehyde (PFA) and embedded in OCT (VWR Chemicals). Four μm sections were mounted on slides. Formalin-fixed paraffin-embedded (FFPE) sections were stained with hematoxylin and eosin (Merck) and images were acquired with a Nikon microscope, equipped with a QImaging digital camera. The ImageJ software was used for measuring tumor size. Sections from OCT-embedded tissues were left to dry, washed with PBS and covered with mounting medium containing DAPI (Sigma). Images were acquired with the TCS SP8X White Light Laser confocal system (Leica).

For immunohistochemistry, FFPE sections were de-paraffinized with Xylene and hydrated in 100% and 70% ethanol. Antigen retrieval was performed using heat-mediated Citrate buffer (pH 6.0) for 20 minutes and slides were allowed to cool down. Slides were then incubated at room temperature in 3% hydrogen peroxidase in PBS for 15 minutes to block endogenous peroxidase activity. Tissue sections were washed and blocked with 1% BSA in PBS for 1 hour and incubated with the primary antibody against phospho-STAT3 (Cell Signaling) overnight at 4°C. A secondary biotinylated antibody against rabbit IgG (Vector) was added for 1 hour at room temperature, followed by the Vectastain ABC kit for 30 minutes at room temperature and peroxidase activity was visualized using ImmPACT DAB Peroxidase (HRP) Substrate (Vector Laboratories). The sections were counterstained with hematoxylin (Merck), dehydrated by incubation in 70% and 100% ethanol, permeated with xylene and preserved in mounting medium (Sigma). For analysis of proliferation and apoptosis, FFPE sections were stained using the BrdU proliferation kit (BD Biosciences) and the DeadEnd Fluorometric Tunel assay (Promega), respectively, according to manufacturer's instructions. Hematoxylin and DAPI (Sigma) were used for counterstain, respectively. For assessment of proliferation, 100mg/ml BrdU (Roche) was administered via i.p. injection 90min before sacrifice. The number of BrdU and Tunel positive cells was quantified in size-matched tumors.

FACS analysis and Cell Sorting

For FACS analysis a part of the small intestine or tumors were removed, washed with HBSS (GIBCO), containing antibiotic-antimycotic solution (GIBCO) and cut into pieces. Intestinal pieces or minced tumors were digested using 400 U/ml Collagenase IV (Sigma-Aldrich), 1 mg/ml Dispase II (Roche) and 100 U/ml Dnase I (Sigma-Aldrich) in DMEM for 40-60 minutes at 37°C. The cell suspension

was centrifuged, resuspended in FACS buffer (PBS with 2% FBS) and cells were counted. The anti-Fc Receptor (anti-CD16/32) antibody (Biolegend) was used to prevent non-specific binding. For stainings, 1-2 million cells were incubated with the following antibodies: FITC-conjugated anti-CD11b (eBioscience), APC/Cy7-conjugated or A700-conjugated anti-CD45 (Biolegend), PE/Cy7-conjugated anti-CD11c (Biolegend), A700-conjugated anti-CD19 (eBioscience), A700-conjugated anti-CD4 (eBioscience), APC-conjugated anti-CD8 (Biolegend), A647-conjugated anti-Gr1 (Biolegend), PE-conjugated anti-F4/80 (eBioscience) and streptavidin-conjugated A750 (Invitrogen) (see Key Resources Table). Propidium iodide (PI) was used for live/dead exclusion (Sigma). Analysis was performed using a FACS Canto II Flow cytometer (BD Biosciences) and FACSDiva (BD Biosciences) or FlowJo software (FlowJo, LLC). Cultured cells were used for sorting based on their GFP and Tomato fluorescent protein expression, using a FACSAria III Cell Sorter (BD Biosciences).

ELISA

Supernatants were collected at 24h and IL-6 quantification was performed using the mouse IL-6 Duo-Set ELISA kit, according to the manufacturer's instructions (R&D Systems).

RNA Isolation and qRT-PCR

RNA was isolated from tumors, intestinal tissue or intestinal mesenchymal cells using the RNeasy mini or micro kit (QIAGEN), according to the manufacturer's instructions. Isolated RNA was subsequently used either for 3′RNA-seq sequencing and analysis, or for construction of cDNA, using the MMLV Reverse Transcriptase (Promega), according to the manufacturer's instruction. The cDNA was subsequently used for qRT-PCR using the Platinum SYBR-Green qPCR SuperMix (Invitrogen) and the CFX96 Touch Real-Time PCR Detection System (Biorad). Quantification was performed with the DDCt method. Primer sequences (5′-3′) are provided (see Table S1).

3′ RNA-Seq sequencing

The quantity and quality of RNA samples were analyzed using Agilent RNA 6000 Nano kit with the bioanalyzer from Agilent. RNA samples with RNA Integrity Number (RIN) > 7 were used for library construction using the 3′ mRNA-Seq Library Prep Kit Protocol for Ion Torrent (QuantSeq-LEXOGEN^{TM}) according to manufacturer's instructions. DNA High Sensitivity Kit in the bioanalyzer was used to assess the quantity and quality of libraries, according to the manufacturer's instructions (Agilent). Libraries were then pooled and templated using the Ion PI^{TM} IC 200 Kit (ThermoFisher Scientific) on an Ion Proton Chef Instrument or Ion One Touch System. Sequencing was performed using the Ion PI^{TM} Sequencing 200 V3 Kit and Ion Proton PI^{TM} V2 chips (ThermoFisher Scientific) on an Ion ProtonTM System, according to the manufacturer's instructions.

QUANTIFICATION AND STATISTICAL ANALYSIS

Analysis of RNaseq data

Mapping of sequencing reads to reference genome was performed as recommended by the manufacturer and gene differential expression analysis was performed using Bioconductor package DESeq through metaseqR pipeline, as previously described (Moulos and Hatzis, 2015). Downstream bioinformatics analysis was performed using InteractiveVenn for Venn diagrams (http://www.interactivenn.net) (Heberle et al., 2015) and the Functional Annotation tool from DAVID for Gene Ontologies (https://david.ncifcrf.gov/) (Huang et al., 2009a, 2009b), while volcano plots and heatmaps were generated in R using an in-house developed script and packages ggplot and gplots (R Core Team, 2017; Warnes et al., 2016; Wickham, 2016).

Datasets and Statistical analysis

The public datasets GEO: GSE39395 and GSE35602 was analyzed using the Geo2R function from NCBI. For Figure 3B, values with the lowest adjusted p value were selected for each gene. For Figure 4F, genes with adjusted p value $\leq$ 0.05 and log2 fold change $\geq$ 1 were used for downstream analysis.

The Student's t test was used to calculate statistical significance for samples that showed normal distribution and the Mann Whitney test for those that did not pass the normality test. Equal variance was evaluated by the F-test. One-way ANOVA, corrected using Tukey test, was used for multiple comparisons. Information on the value of n, what n represents, the definition of center and dispersion and precision measures can be found in the Figure legends. Mouse sample size was estimated by power analysis. Data were analyzed with GraphPad Prism 6. p values $\leq$ 0.05 were considered significant.

DATA AND SOFTWARE AVAILABILITY

RNA-seq datasets are accessible through GEO: GSE119341 of NCBI's Gene Expression Omnibus.

Cell Reports, Volume *26*

Supplemental Information

Innate Sensing through Mesenchymal TLR4/MyD88 Signals Promotes Spontaneous Intestinal Tumorigenesis

Vasiliki Koliaraki, Niki Chalkidi, Ana Henriques, Christos Tzaferis, Apostolos Polykratis, Ari Waisman, Werner Muller, David J. Hackam, Manolis Pasparakis, and George Kollias

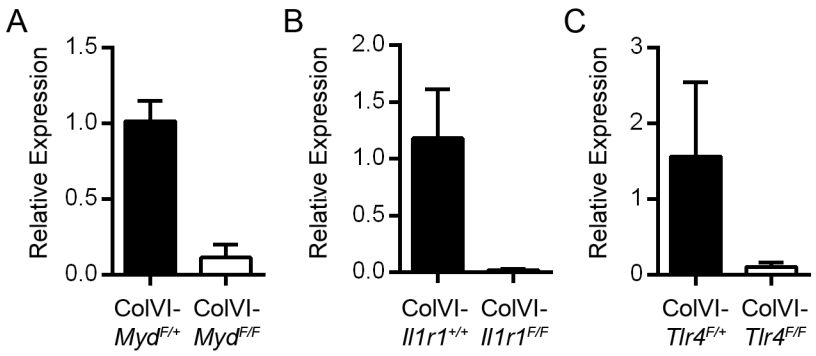

Figure S1. Deletion efficiency of *Myd88*, *Il1r1* and *Tlr4*. Related to Figures 1 and 3. qRT-PCR analysis of isolated GFP$^+$ cells from (A) ColVIcre-*Myd88*$^{F/+}$-mTmG and ColVIcre-*Myd88*$^{F/F}$-mTmG, (B) ColVIcre-*Tlr4*$^{F/+}$-mTmG and ColVIcre-*Tlr4*$^{F/F}$-mTmG and (C) ColVIcre-*Il1r1*$^{+/+}$-mTmG and ColVIcre-*Tlr4*$^{F/F}$-mTmG. B2m was used for normalization (n=3).

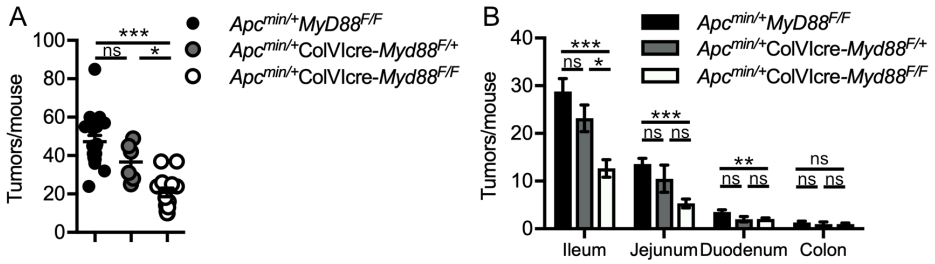

Figure S2. Cre in the *Apc*$^{min/+}$-*Myd88*^{IMCko} does not affect tumor development. Related to Figure 1. (A) Total number of tumors per mouse and (B) number of tumors per intestinal part in 4-month old *Apc*$^{min/+}$ColVIcre-*Myd88*$^{F/F}$ (n=15), *Apc*$^{min/+}$ColVIcre-*Myd88*$^{F/+}$ (n=6) mice and their littermate controls (n=18). Data represent mean ± SEM. *p<0.05, **p<0.01, ***p<0.001, ns = not significant.

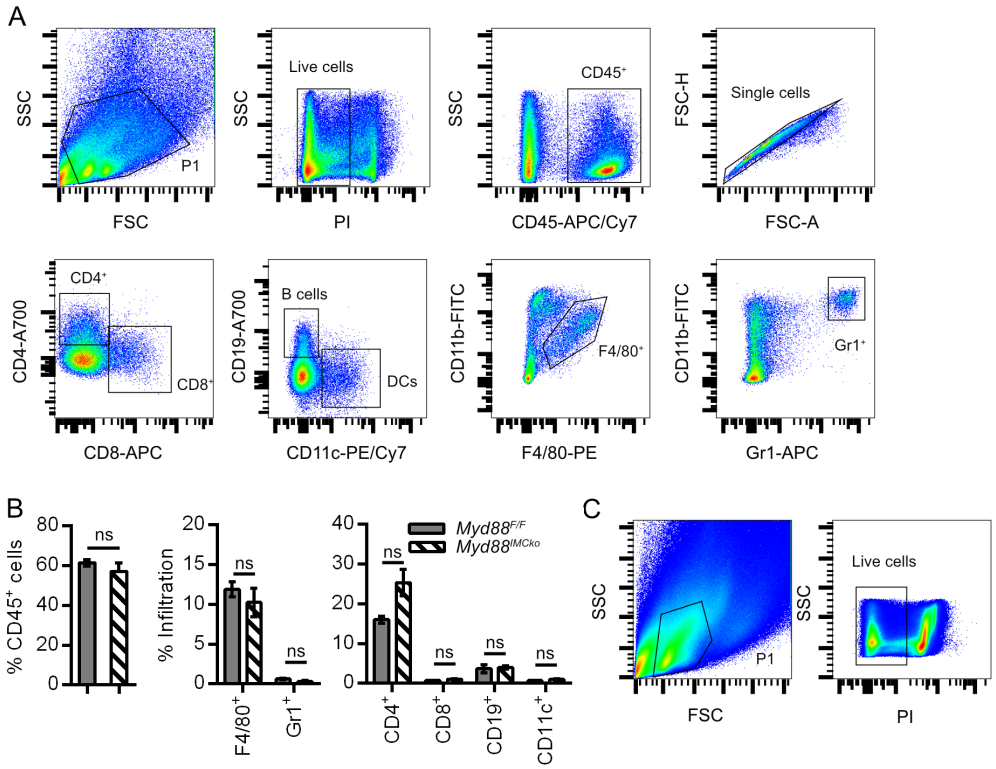

Figure S3. FACS gating strategies. Related to Figure 2. (A) FACS gating strategy for measuring inflammatory cell infiltration in the small intestine and tumors. The cell suspension was gated for live CD45$^+$. In this CD45$^+$ population, we plotted CD4 and CD8, for measuring the respective T cell populations, CD19 and CD11c for B and dendritic cell and CD11b with F4/80 and Gr1 to identify double positive CD11b$^+$F4/80$^+$ and CD11b$^+$Gr1$^+$ cells. (B) Infiltration of CD45$^+$ cells, CD11b$^+$F4/80$^+$ macrophages, CD11b$^+$Gr1$^+$ neutrophils, CD4$^+$ T cells, CD8$^+$ T cells, CD19$^+$ B cells and CD11c$^+$ dendritic cells in intestinal tissue from *Myd88*$^{F/F}$ and *Myd88*^{IMCko} mice or 3-month old *Apc*$^{min/+}$*Myd88*$^{F/F}$ and *Apc*$^{min/+}$*Myd88*^{IMCko} mice (n=4-5), quantified by FACS analysis. Data represent mean ± SEM. ns = not significant. (C) Gating strategy for Figure 2H. Single-cell suspensions from tumors were gated for live cells using Propidium Iodide (PI) (n=3 mice).

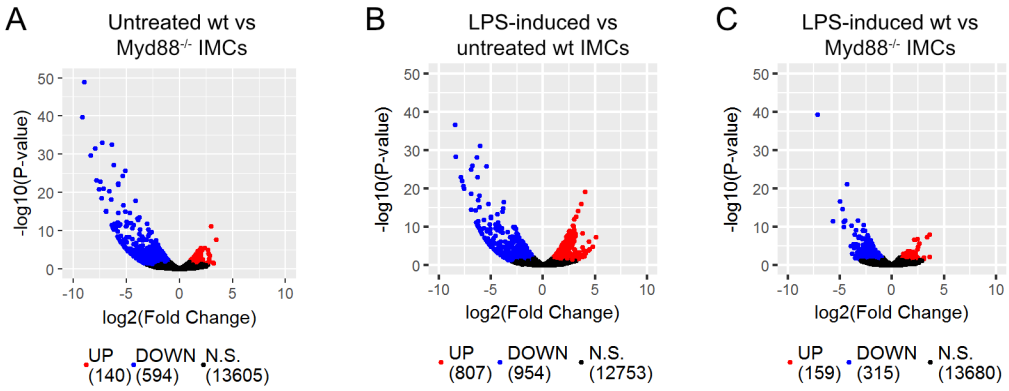

Figure S4. Comparisons between samples used for RNA sequencing. Related to Figure 4. (A) Volcano plot of deregulated genes between untreated wt and MyD88$^{-/-}$ IMCs. (B) Volcano plot of deregulated genes between untreated and LPS-treated wt IMCs. (C) Volcano plot of deregulated genes between LPS-treated wt and MyD88$^{-/-}$ IMCs. Not significant genes are depicted with black color (N.S), significant up regulated genes (p-value < 0.05, log2FC > 1) with red and significant down regulated genes (p-value < 0.05, log2FC < -1) with blue.

Table S1. List of primers for qRT-PCR. Related to STAR Methods.

Gene	Primer (5'-3')	Size (bp)	Anneal. Tem.	Reference
Ptgs2	F: TGAGCACAGGATTTGACCAG R: CCTTGAAGTGGGTCAGGATG	150	58	(Salcedo et al., 2010)
Il6	F: GTTCTCTGGGAAATCGTGGA R: TCCAGTTTGGTAGCATCCATC	138	59	(Salcedo et al., 2010)
Il11	F: AACTGTGTTTGTCGCCTGGT R: CGTCAGCTGGGAATTTGTCT	199	59	(Salcedo et al., 2010)
Cd44	F: TTATCCGGAGCACCTTGGCCAC R: TGCACTCGTTGTGGGCTCCTGAG	143	59	
Tnf	F: CACGCTCTTCTGTCTACTGA R: ATCTGAGTGTGAGGGTCTGG	110	55	
Mmp7	F: GCTGCCACCCATGAATTTGGCC R: GGACCCAGTGAGTGCAGACCG	209	59	
Cxcl1	F: CGCACGTGTTGACGCTTCCC R: TCCCGAGCGAGACGAGACCA	105	59	
Igf1	F: GGGAGATGCAAAGGCCTCCCC R: ACCAGGACTCCCAAATCCCTAGCC	142	56	
Igfbp5	F: ACGGCGAGCAAACCAAGATA R: GAGGGCTTACACTGCTTTCT	382	55	(Ding et al., 2016)
Mmp10	F: CACAAGCCCAGCTAACTTCC R: TTTGTCTGGGGTCTCAGGTC	136	59	(Salcedo et al., 2010)
Myd88	F: CTAGGACAAACGCCGGAACT R: ATTAGCTCGCTGGCAATGGA	176	60	
Tlr4	F: TTCAGAACTTCAGTGGCTGGAT R: GTCTCCACAGCCACCAGATT	177	58	
Il1r1	F: ACAACGTGAGCTTCTTCGGA R: GCTTCCCCCGGAACGTATAG	108	60	
B2m	F: TTCTGGTGCTTGTCTCACTGA R: CAGTATGTTCGGCTTCCCATTC	104	58	
Hprt	F: TGCCGAGGATTTGGAAAAAGTG R: CACAGAGGGCCACAATGTGATG	116	55	